Multiscale Statistical Properties of a High-Resolution Precipitation Forecast

DANIEL HARRIS AND EFI FOUFOULA-GEORGIOU

St. Anthony Falls Laboratory, University of Minnesota, Minneapolis, Minnesota

KELVIN K. DROEGEMEIER

Center for Analysis and Prediction of Storms, and School of Meteorology, University of Oklahoma, Norman, Oklahoma

JASON J. LEVIT

Center for Analysis and Prediction of Storms, University of Oklahoma, Norman, Oklahoma

(Manuscript received 15 June 2000, in final form 24 March 2001)

ABSTRACT

Small-scale (less than ~15 km) precipitation variability significantly affects the hydrologic response of a basin and the accurate estimation of water and energy fluxes through coupled land–atmosphere modeling schemes. It also affects the radiative transfer through precipitating clouds and thus rainfall estimation from microwave sensors. Because both land–atmosphere and cloud–radiation interactions are nonlinear and occur over a broad range of scales (from a few centimeters to several kilometers), it is important that, over these scales, cloud-resolving numerical models realistically reproduce the observed precipitation variability. This issue is examined herein by using a suite of multiscale statistical methods to compare the scale dependence of precipitation variability of a numerically simulated convective storm with that observed by radar. In particular, Fourier spectrum, structure function, and moment-scale analyses are used to show that, although the variability of modeled precipitation agrees with that observed for scales larger than approximately 5 times the model resolution, the model shows a falloff in variability at smaller scales. Thus, depending upon the smallest scale at which variability is considered to be important for a specific application, one has to resort either to very high resolution model runs (resolutions 5 times higher than the scale of interest) or to stochastic methods that can introduce the missing small-scale variability. The latter involve upscaling the model output to a scale approximately 5 times the model resolution and then stochastically downscaling it to smaller scales. The results of multiscale analyses, such as those presented herein, are key to the implementation of such stochastic downscaling methodologies.

1. Introduction

The numerical simulation of precipitation at high spatial resolution (1–10 km) has undergone a period of rapid development over the last decade as a result of the increasing computational power of massively parallel computers and substantial improvements in the collection and assimilation of high-resolution observations of the atmosphere [e.g., satellite, Weather Surveillance Radar-1988 Doppler (WSR-88D), and ground-based in situ networks; e.g., Droegemeier (1997)]. Of great interest are the hydrological applications of these numerical forecasts for flood prediction over small- to medium-sized basins (a few to several hundred square kilometers), as recently discussed by the U.S. Weather Research Program Prospectus Development Team Nine (Droegemeier et al. 2000). Another application involves the use of 3D numerically simulated cloud fields in Bayesian inversion algorithms used to estimate rainfall from satelliteborne passive microwave radiometers (Kummerow et al. 1996; Kummerow and Giglio 1994).

In these and other applications, the modeled precipitation variability over a wide range of scales is important. For example, studies of the effect of precipitation variability on basin response (e.g., Ogden and Julien 1993, 1994; Winchell et al. 1998) suggest that runoff volume is sensitive to the small-scale spatial and temporal variability of the precipitation field, which is provided as input to a rainfall–runoff model. The specific study of Winchell et al. (1998) found systematic and significant decreases in simulated infiltration–excess runoff volume as the spatial resolution of the radar-estimated precipitation fields was decreased from 1 to 16 km. Another example of the importance of small-scale (less than 10 km) precipitation variability is provided by the coupled land–atmosphere modeling study of Nykanen et al. (2001), in which the inclusion of

Corresponding author address: Efi Foufoula-Georgiou, University of Minnesota, St. Anthony Falls Laboratory, Mississippi River at 3d Ave. S.E., Minneapolis, MN 55414.
E-mail: efi@tc.umn.edu

subgrid rainfall variability at scales as small as 3 km was found to propagate to larger-scale (greater than 20–30 km) anomalies in soil moisture, ground temperature, and surface runoff, as well as sensible and latent heat fluxes.

The importance of modeled precipitation and cloud variability for inversion algorithms used to estimate precipitation from passive microwave radiometer measurements has been addressed in a number of studies (e.g., Kummerow et al. 1996; Kummerow and Giglio 1994; Spencer 1986; Harris and Foufoula-Georgiou 2001) and is generally referred to as the beam-filling problem. In essence, simulated precipitating cloud fields are used together with radiative transfer schemes to simulate how a microwave radiometer would observe a real storm. The computed microwave radiances are used to create a large database of precipitation–radiance pairs at a resolution comparable to the footprint of the microwave radiometer. The database forms the input to a Bayesian inversion algorithm, which is used to relate observed radiance to likely precipitation. Given the nonlinear relationship between precipitation and the upwelling microwave radiance, a microwave radiometer (which linearly averages the microwave radiance over the scale of the radiometer's footprint) necessarily performs a nonlinear averaging of precipitation. For this reason, the precipitating cloud fields are simulated at resolutions higher than the footprint of the radiometer so as to capture the small-scale variability and thus the higher statistical moments, which considerably affect the nonlinear averaging.

Atmospheric numerical models are expected to underrepresent the small-scale spatial variability of precipitation because their associated finite-difference computational fluid dynamical schemes contain smoothing in the form of both implicit and explicit numerical diffusion, as well as physically based subgrid-scale turbulent mixing. Implicit diffusion, which arises from the combined effects of truncation error–generated dissipation and dispersion, is a fundamental characteristic of finite-difference schemes and is dependent upon grid resolution. Higher-order and nonlinear (e.g., monotonic, flux corrected, and positive definite) schemes tend to be less dispersive than their low-order counterparts, though they are computationally much more expensive.

Explicit numerical diffusion (also referred to here as computational smoothing) arises by virtue of a small damping term, typically proportional to the second- or fourth-order partial derivative (with respect to the coordinates) of a scalar (e.g., rain) or dynamical (e.g., velocity) quantity that is added to the conservation equations to counter nonlinear instability. As a rule, this damping is designed to act upon only the smallest resolvable scales (at which the partial derivatives are large) up to a factor of approximately 6–8 Δx, where Δx represents the spatial resolution of the model. Such smoothing reduces the small-scale variability of both dynamic and scalar fields and, in some cases, can have a significant impact on solution energetics (e.g., Lilly and Jewett 1990).

Subgrid-scale turbulent mixing has essentially the same effect in reducing variability as computational smoothing, though it is designed to represent, in a statistical manner, the physical effects of turbulent motions unresolvable by the grid. Thus, although its effects are more selective (e.g., the mixing is activated only in regions for which specific instability criteria are met, with the mixing of scalar and momentum fields typically occurring at different rates), it too reduces the small-scale variability of both dynamic and scalar fields.

The falloff in variability in modeled precipitation as a result of both physically based (turbulent mixing) and computational mixing manifests itself in the apparent smoothness of fields in comparison with observations and can be noticed visually. For example, Fig. 1 compares the base reflectivity observed from a WSR-88D radar (radar data processing and field estimates are discussed in the following section) with that predicted by a 3D numerical cloud model. The modeled field is seen to be less intermittent and smoother in the rainy areas than its radar counterpart. Therefore, although one expects a discrepancy in variability between observed and modeled precipitation, a key question remains to be answered—how large is the discrepancy, and over what range of scales does it occur?

To characterize and to quantify better the scale dependence of precipitation spatial variability, a suite of multiscale statistical techniques is used in this study. To be specific, the simulated and radar-observed rain liquid water (RLW) fields just above the ground are compared via their respective spatial Fourier spectra, structure functions, and moment-scale functions. These functions are easily computable and have conceptually accessible physical interpretations (which are elaborated upon below), allowing an understanding of the spatial structure of the fields over a wide range of scales. Also, the use of multiscale functions allows one to identify the range of scales over which the scale dependence of modeled variability may deviate from the scale dependence of observed variability and the range of scales over which the two agree. The choice of these methods to characterize the statistical variability of precipitation is also influenced by the fact that they allow the development of cascade-based stochastic downscaling methodologies [first applied to simulated fields by Wilson et al. (1991)] by which modeled precipitation fields can be disaggregated spatially to yield high-resolution fields with realistic variability [e.g., see Harris and Foufoula-Georgiou (2001) for a microwave remote sensing application of wavelet-based stochastic downscaling].

The idea of analyzing observed and modeled precipitation over multiple scales was first explored in Zepeda-Arce et al. (2000) for the purposes of quantitative precipitation forecast (QPF) verification. The underlying premise of that study was that discrepancies between the multiscale statistical structure and dynamics of mod-

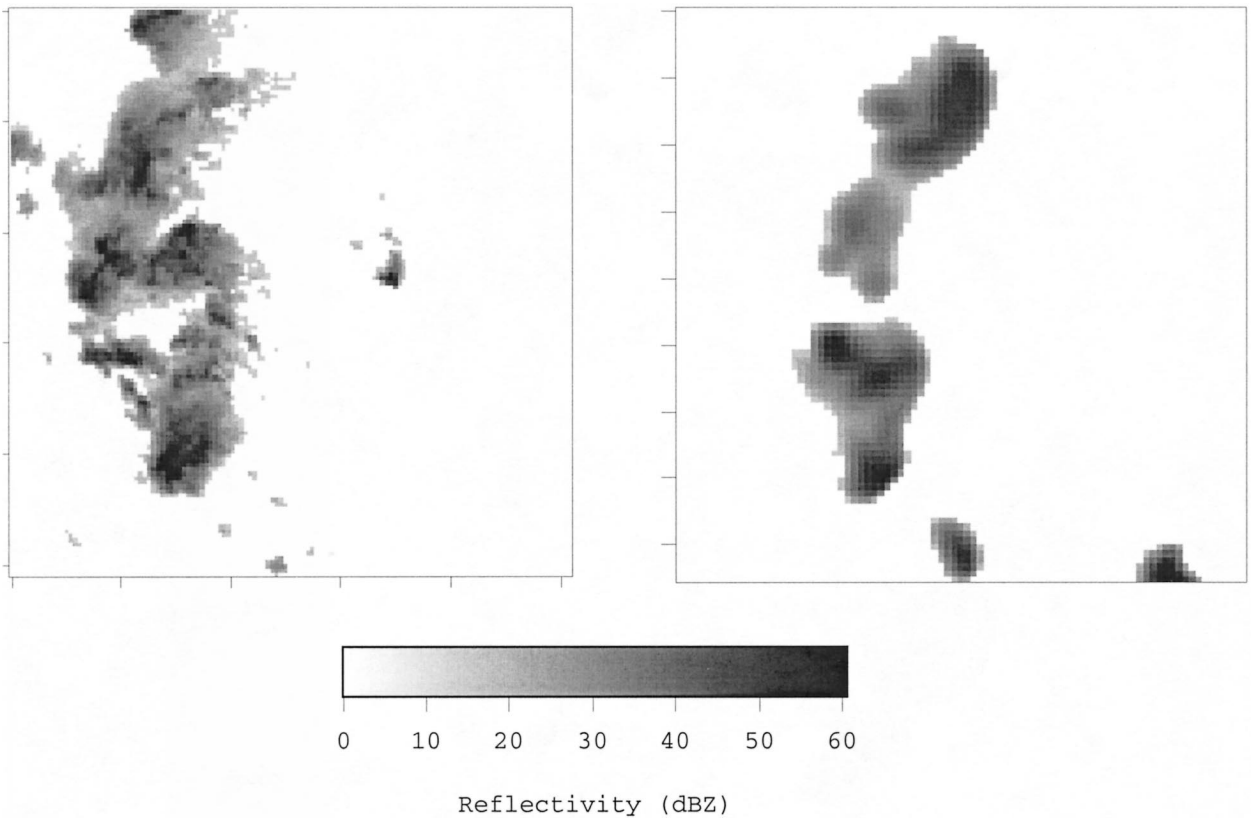

FIG. 1. Visual comparison of (left) radar base-scan reflectivity with its (right) ARPS-forecast counterpart for a southern plains storm on 3 Jun 1999. The radar image (NEXRAD-KAMA) is from 0010 UTC 3 Jun. The horizontal extent of each image is 256 × 256 km^2. The radar image has 2-km resolution, and the forecast has 3-km resolution. Note the visually smoother, more spatially organized structure of the forecast field.

el-predicted and observed precipitation could shed light on the sources of model shortcomings and systematically guide model improvements in terms of physical parameterizations. For that reason, the multiscale methodologies employed were centered around certain measures previously shown to have promise in relating statistical to physical properties of precipitation (Perica and Foufoula-Georgiou 1996a). Specifically, the analysis in Zepeda-Arce et al. (2000) was based on the rate of growth of variance of standardized spatial rainfall fluctuations with scale (e.g., Perica and Foufoula-Georgiou 1996b) and on the presence of dynamic scaling in the spatiotemporal structure of rainfall (e.g., Venugopal et al. 1999). A 6-km precipitation forecast was compared with 4-km radar-observed precipitation. Because both methodologies used in that study employed discrete orthogonal wavelet decomposition with dyadic changes in scale, only comparisons of normalized rainfall gradients at scales of 12 to 48 km (the upper limit imposed for statistical considerations) were possible. In the current study, a higher-resolution precipitation forecast (3 km) is analyzed, and the methods of analysis allow direct interpretation of the variability of rainfall intensities themselves at scales as small as 3 km. In addition, they allow the development of an alternative stochastic downscaling methodology (based on multiplicative cascades) to reintroduce the missing small-scale variability for applications for which it is deemed necessary.

It is noted that the multiscale methodologies employed in Zepeda-Arce et al. (2000) and also in this paper are insensitive to phase errors (large time or spatial lags in the space–time location of the storm). This is important because even a ''perfect'' forecast, except lagged by a few minutes in time or a few kilometers in space, can result in poor performance according to the traditional indices of performance such as bias, rmse, and threat score. Although capturing the location, timing, and intensity of storms is of unquestionable importance for flood estimation, there are applications such as the microwave-based rainfall estimation algorithm discussed earlier for which the issue of space–time location of the storm is of little relevance. Furthermore, as was argued in Zepeda-Arce et al. (2000), missing the location of the storm versus not reproducing its multiscale variability and dynamics points to different shortcomings in the physical parameterizations of the model. As a consequence, there exist advantages in pursuing both traditional and multiscale verification procedures.

In this study, no attempt is made to optimize the model (in terms of initial conditions and data assimi-

lation) to reproduce the exact morphology of the storm. As a result, a temporal phase error of 3 h is present between the predicted and observed storm owing to the model's time lag in initiating convection. After the convection was initiated, however, the modeled storm developed very similarly to the observed in terms of precipitation amount, rate, and general structure. Because the focus of this study is on the question of whether the multiscale variability of the observed storm was reproduced in the model, analysis of the traditional statistics such as bias and rmse, which are influenced by the aforementioned temporal phase error, is not reported. However, other studies have addressed issues of the Advanced Regional Prediction System (ARPS) model validation and forecast accuracy using more conventional statistics (Hou et al. 2001; Miller 2000).

This paper is structured as follows. The numerical weather prediction model used in this study is described briefly in the next section, along with the radar data used to provide the observed fields. The analysis techniques and results are presented in section 3, and the implications of the similarities and differences between modeled and observed fields are discussed in the summary and conclusions (section 4).

2. Model and dataset

a. The Advanced Regional Prediction System (ARPS)

The numerical model used in this study is ARPS, developed at the Center for Analysis and Prediction of Storms (CAPS), University of Oklahoma. As the name suggests, ARPS is more than a cloud model. It is a complete numerical prediction system that incorporates many advances in data assimilation developed at CAPS with particular emphasis on the use of Doppler radar data for model initialization. ARPS is currently providing real-time forecasts at horizontal resolutions as high as 3 km (at the time of writing, examples could be found online at http://caps.ou.edu/wx/aa). Details of the ARPS model may be found in Xue et al. [1995 (http://caps.ou.edu/ARPS/ARPS4.guide.html), 2000, 2001).

ARPS, like most other cloud models and mesoscale models, is physically based and operates on finite-difference representations of the Navier–Stokes equations and thermodynamic and microphysical processes [a six-category water–ice microphysical parameterization scheme (Lin et al. 1983) was used]. One might thus expect such cloud-resolving models to reproduce closely the variability found in observed fields. However, this often is not the case over the full range of modeled scales for the reasons concerning computational smoothing and subgrid turbulent mixing discussed in the previous section.

The ARPS forecast used in this study employed a fourth-order computational mixing scheme, which adds to the conservation equations a small term proportional to the fourth-order partial derivatives of the perturbation of a field quantity from its base-state value. The proportionality constants (K_h for the horizontal and K_v for the vertical) in this additive term are the computational diffusion coefficients (e.g., Pielke 1984; Xue et al. 1995), the values of which in this study were set to $K_h = 4.86 \times 10^{10}$ m^4 s^{-1} and $K_v = 1.536 \times 10^7$ m^4 s^{-1}.

b. Case description and forecast model configuration

Version 4.4 of ARPS was used to forecast the initiation and subsequent evolution of a line of convection that developed in eastern New Mexico on 2 June 1999 in response to forcing associated with a well-defined dryline. By 0000 UTC 3 June, the line was located in the western Texas Panhandle, and, during the subsequent 6 h, the convective system moved slowly eastward until it began to dissipate in western Oklahoma.

ARPS was configured using three computational grids, as shown in Fig. 2a: a continental U.S. grid of 32-km resolution (grid A), a nested 9-km grid (grid B), and a nested 3-km grid (grid C). A schematic indicating the initialization times and run times of the forecasts over the three different domains is depicted in Fig. 2b. The 36-h forecast on grid A was initialized at 1200 UTC on 2 June 1999 using the National Centers for Environmental Prediction Eta Model 12-h forecast as the background field, to which were assimilated, via the ARPS Data Analysis System (Brewster 1996), Geostationary Operational Environmental Satellite data, surface observations, rawinsonde, and wind profiler observations. Boundary conditions for grid A were supplied by the Eta forecast, interpolated in time and space to the ARPS grid.

The 15-h ARPS forecast on grid B, which was one-way nested within grid A, was initialized at 1500 UTC 2 June 1999 using the 3-h forecast from grid A as the background state, to which were assimilated surface, satellite, and wind profiler observations. In addition, Next-Generation Weather Radar (NEXRAD) Information Dissemination Service reflectivity data from 30 radars were also assimilated at the start of the forecast to provide storm-scale moisture and diabatic heating fields. The 6-h grid-C forecast, one-way nested within grid B, was initialized at 0000 UTC 3 June 1999 using the 9-h grid-B forecast, valid at 0000 UTC, as the background field. Level-II (base scan) WSR-88D data from the radars at Fort Worth, Texas, Tulsa, Oklahoma, and Fort Smith, Arkansas—acquired as part of the Collaborative Radar Acquisition Field Test (Droegemeier et al. 1999)—were assimilated into the grid-C forecast domain using the ARPS single-Doppler velocity retrieval (SDVR) system (Shapiro et al. 1995; Weygandt 1998). To be specific, the azimuthal and polar wind components were retrieved from time series of radial velocity data, and from this 3D wind field the temperature and pressure fields were also retrieved. Data assimilation is a major component of ARPS, and, in particular, the use of Level-II NEXRAD data has been shown to aid forecast ac-

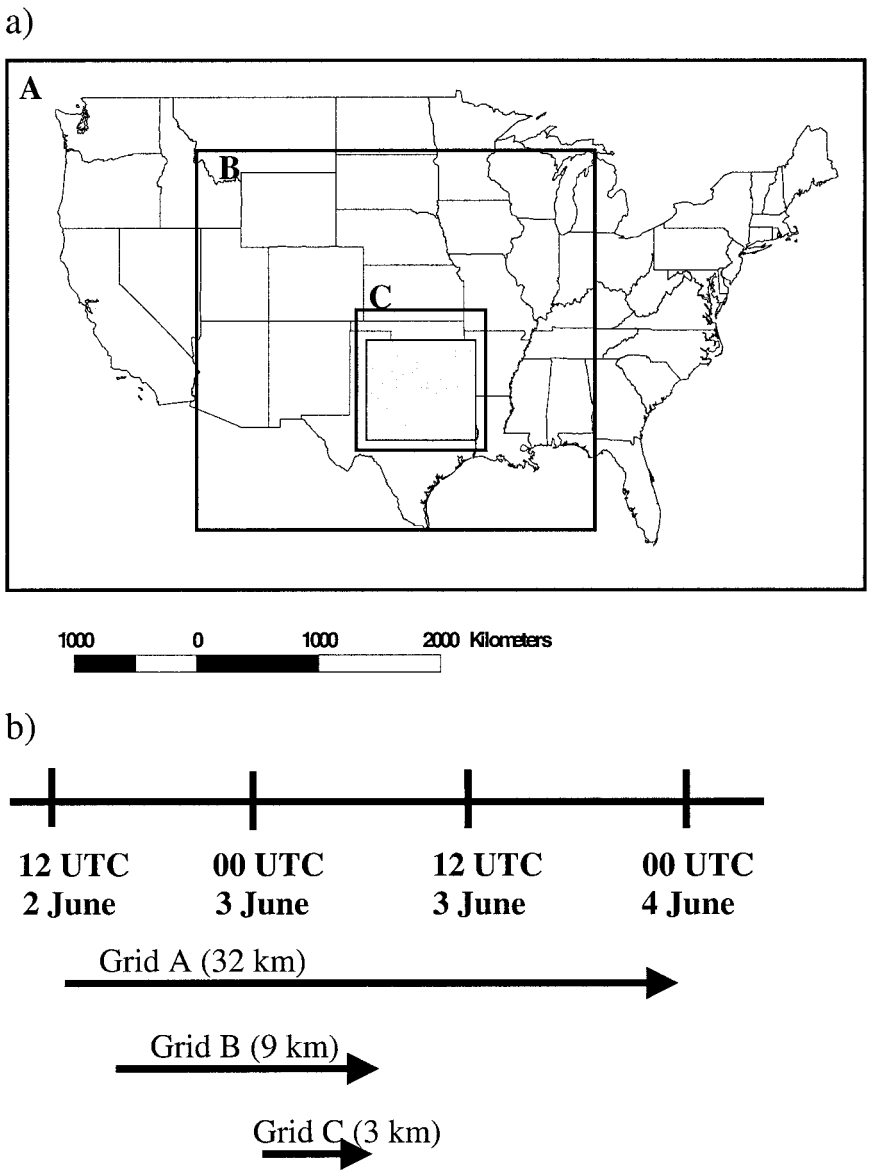

FIG. 2. (a) Map showing forecast domains and study region and (b) time line for the three forecasts having different resolution. The largest region, grid A, represents the continental U.S. model run at 32-km spacing over an area of 5120 × 3520 km². Nested within grid A are regions for the 9-km run (grid B, 2295 × 2295 km²) and the 3-km run (grid C, 855 × 945 km²). The shaded study region is a 768 × 768 km² subdomain of grid C.

curacy significantly (Droegemeier et al. 1999). Level-II data unfortunately were not available for assimilation from the Amarillo and Lubbock, Texas, radars.

Each of the ARPS computational grids used 53 levels in the vertical, with a vertical grid interval that stretched continuously from 20 m at ground to 740 m at an altitude of 20 km. Model output from grid C was saved to disk every 5 min for use in the multiscale statistical analysis. The domain of study is shown by the shaded region in Fig. 2a, corresponding to a 768 × 768 km² (256 × 256 pixel) region.

c. WSR-88D data

Level-II (base scan) WSR-88D data from the Amarillo (KAMA) radar were available for the storm described above from about 2200 UTC 2 June to 0100 UTC 3 June 1999 for purposes of comparison with the model output (as mentioned above, the Amarillo Level-II data were not available for assimilation using the SDVR system). Constant-altitude plan position indicator (CAPPI) maps were made from the lowest two elevations, corresponding to four scans given that the ra-

dar scanned at the lowest two elevations (~0.5° and ~1.5°, respectively) twice. The CAPPIs were then rasterized at 2-km horizontal resolution to form 256 × 256 km² images (128 × 128 pixels; see Fig. 1a) every 5 min for the entire radar dataset.

RLW concentration q_r (g m^{-3}) was estimated from reflectivity Z following Kessler (1969):

$$q_r = aZ^b, \tag{1}$$

where

$$a = (1.73 \times 10^4)^{-b} \quad \text{and} \quad b = 4/7. \tag{2}$$

The peak reflectivity was marginally over 60 dBZ, indicating the presence of hail, so an upper-bound reflectivity threshold of 53 dBZ was applied. A lower-bound threshold of 25 dBZ was applied corresponding to an RLW concentration of 0.1 g m^{-3}. The specific values of the upper and lower bounds chosen do have, in some instances, an effect on the results of the multiscale analysis below, although the effect was usually small. Sensitivity to these bounds was examined in the analysis by varying the lower bound between 15 and 25 dBZ and the upper bound between 50 and 60 dBZ. The sensitivities are mentioned together with the respective results of each analysis method in the following section.

3. Multiscale statistical analysis

Three methods of multiscale statistical analysis were used in this study: Fourier power spectrum, generalized structure function, and moment-scale analysis. Each method is described briefly and its physical interpretation is given prior to the results of the analysis. Results are presented in this paper for a 1-h sequence of observed and simulated images (1 h being approximately the time for which the entire storm was in the field of view of the radar). An overview and an integration of the findings from the three methods are presented in section 4.

a. Spatial Fourier power spectra

A simple tool for studying the variability of any field over a wide range of scales is the Fourier power spectrum. The power spectrum is computed using standard 2D FFT algorithms such as those found in Press et al. (1992). The Fourier power or energy spectrum $E(k_x, k_y)$ of any 2D field such as RLW is found by multiplying the 2D FFT by its complex conjugate, where k_x and k_y are the wavenumber components. To facilitate visualization and comparison, the 2D power spectra from the fields are averaged angularly about $k_x = k_y = 0$ to yield what is referred to here as the isotropic energy spectrum E(k), with $k = (k_x^2 + k_y^2)^{1/2}$. The term isotropic energy spectrum is not to suggest that the field is isotropic but rather that the angular averaging about $k_x = k_y = 0$ integrates the anisotropy, thus facilitating comparisons.

An empirical observation often (but not always) noted for a wide variety of atmospheric fields is the presence of scaling or scale invariance, which manifests itself as log–log linearity of the power spectrum in space or time:

$$E(k) \sim k^{-\beta}. \tag{3}$$

Evidence of scaling power spectra for rain fields in both space and time can be found in numerous studies (e.g., Harris et al. 1996; Menabde et al. 1997; Lovejoy and Schertzer 1995; Georgakakos et al. 1994) as well as for cloud liquid water fields (e.g., Davis et al. 1996b; Lovejoy and Schertzer 1995). The scaling nature of these atmospheric fields is largely empirical, although arguments in the literature suggest that the scaling of observed scalars such as rainwater or cloud water is linked to the scaling observed in turbulence (Schertzer and Lovejoy 1991). The spectral slope β is an indicator of smoothness (e.g., Davis et al. 1996b; Harris et al. 1996), with high spectral slopes characteristic of a smoother, more organized structure. For this specific storm and over the scaling range observed, the full 2D power spectrum is nearly isotropic. For storms for which a high degree of anisotropy is observed over the scaling range, it may be interesting to characterize further the degree of anisotropy by considering directional components of the power spectrum.

The Fourier power spectra of the radar-observed and forecast RLW fields have been computed for each image (every 5 min for the radar and model) and are shown on a log–log plot in Fig. 3 for the image pair shown in Fig. 1. The spectra have been normalized by their respective mean spectral energies. As was expected because of computational smoothing, a falloff in variability at small scales (high wavenumbers) is evident in the modeled field in comparison with the observed field. The scale of this falloff is estimated to be approximately 15 km, which corresponds to 5 times the horizontal resolution of the modeled field. The scaling range for the radar spectrum, shown in Fig. 3, extends to ~30 km and is estimated to have a slope of $\beta \approx 3.0$, which is at the high end of the range of spectral slopes (~1.8 to ~3.0) found for rainfall radar imagery (Menabde et al. 1999). Over the 1-h sequence of images, the estimates for β ranged from 2.7 to 3.1, with a mean of 2.8 ± 0.2. There is some sensitivity of β to the value of the upper bound placed on the reflectivity to account for hail contamination; the lower bound had no effect. Varying the upper bound between 50 and 55 dBZ changed β by ~0.02. However, allowing hail contamination by increasing the upper bound to 60 dBZ lowered β by 0.1 to 0.2, which is comparable to the fit uncertainty (i.e., standard error of the estimate in the least squares fit) and temporal variability of β over the 1-h sequence. Varying the lower bound from 15 to 25 dBZ had no effect on β. The high values of β found here are consistent with the fact that the analyzed storm is convectively driven and thus has a highly organized and smooth spatial structure (Harris et al. 1996). Values of

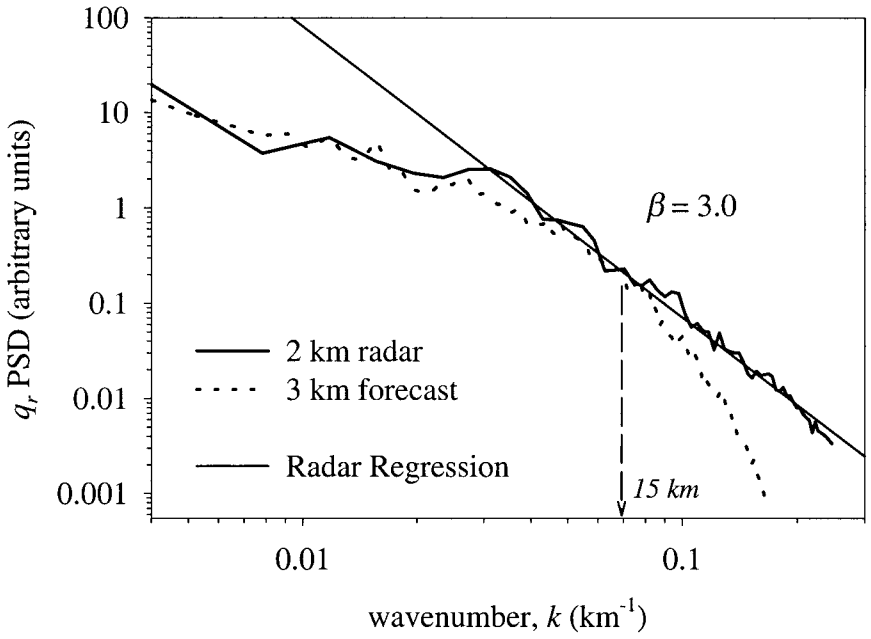

FIG. 3. Isotropic spatial Fourier power spectral density (PSD) for forecast RLW (q_r; dotted line) and radar-observed q_r (solid line). Comparison of the spectra shows reasonable agreement at scales larger than 15 km. For scales smaller than 15 km, the forecast shows a rapid falloff in variability in comparison with the radar. The estimated spectral slope with fit uncertainty is $\beta = 3.0 \pm 0.1$.

β greater than 2 are of importance for the moment-scale analysis discussed later in this section.

b. Generalized structure function

The structure function is a popular alternative to the covariance function when the field being analyzed is (spatially) nonstationary but has stationary increments (e.g., Yaglom 1987). We define the 2D structure function generalized to qth order as.

$$S_q(l_x, l_y) = \langle |R(x + l_x, y + l_y) - R(x, y)|^q \rangle, \quad (4)$$

where R is the field of interest (e.g., RLW), $\langle\ \rangle$ denotes the average over the nonzero pixels in the image, and l_x and l_y are the lags in the x and y directions, respectively. Similar to the Fourier power spectrum, the isotropic structure function was computed by averaging $S_q(l_x, l_y)$ over all angles about $(l_x, l_y) = (0, 0)$, giving $S_q(l)$ where $l = (l_x^2 + l_y^2)^{1/2}$. For q equal to 2, one has the standard semivariogram often used in the earth sciences (e.g., Christakos 1992). Changing the value of q amounts to selecting whether the statistic places emphasis on extreme fluctuations (high q will emphasize these) or smaller fluctuations [low q ($0 < q < 1$) will emphasize these relative to extreme increments].

The physical interpretation of the structure function is as follows. First, one expects that the structure function increases with lag, at least for small scales [i.e., $S_q(0)$ is necessarily 0 and $S_q(l) > 0$ for $l > 0$]. The rate at which $S_q(l)$ increases with l is a measure of the smoothness and degree of organization in the structure of the underlying field. To illustrate, if one considers a totally uncorrelated (white noise) field, increasing lag has little (none in theory) effect on $S_q(l)$, giving a more or less constant value independent of lag ($l > 0$). On the other hand, a highly correlated and smoother field exhibits small $S_q(l)$ for small lag (because nearby points are likely to be very similar in magnitude) but exhibits increasingly greater differences in (4) as lag is increased, causing a steep rise on an $S_q(l)$-versus-l plot.

Scaling in the generalized structure function exists when

$$S_q(l) \sim l^{\zeta(q)}, \quad (5)$$

where $\zeta(q)$ is the structure-function scaling exponent. In general, $\zeta(q)$ is a nonlinear function of q, but for special stochastic processes such as Brownian surfaces it is linear in q. In this study, we focus primarily on $q = 1$ because the value of the exponent $\zeta(1)$ is the Hurst exponent H [e.g., see Davis et al. (1996a) and references therein]. The Hurst exponent plays an important role in the moment-scale analysis below and is elaborated upon in the appendix.

The first-order ($q = 1$) structure functions of the radar-observed and modeled RLW fields in Fig. 1 are shown on a log–log plot in Fig. 4. Again, a comparison shows a steeper curve for the modeled field than the radar RLW field at scales below 10 km, indicating a smoother structure for the former at these scales. The scaling for the observed field shown in Fig. 4 is not excellent, but it is estimated to have a slope, over the range extending up to ~10 km, of $\zeta(1) = H = 0.65$.

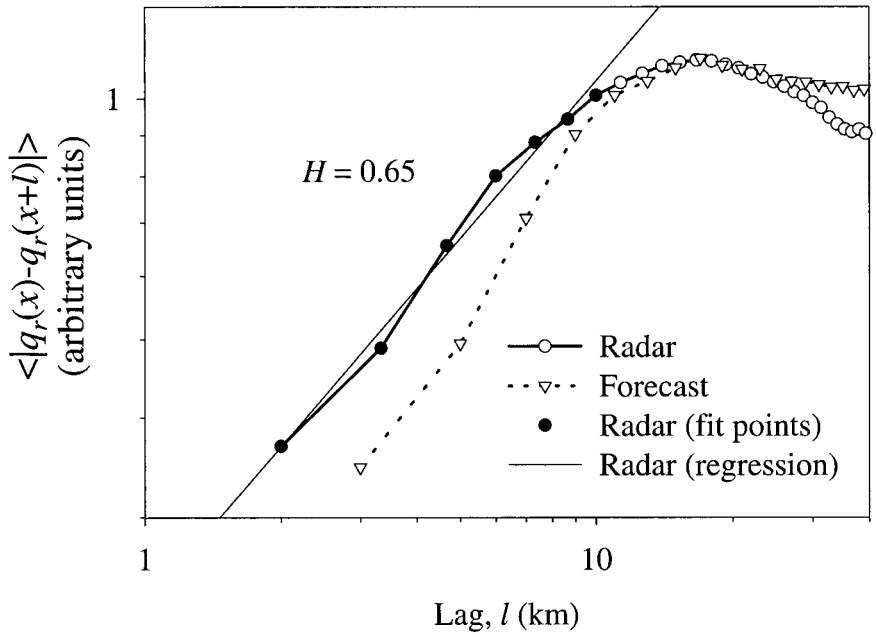

FIG. 4. Isotropic generalized structure function ($q = 1$) for forecast q_r (dotted line–triangles) and radar-observed q_r (solid line–circles). Comparison of the structure functions shows a steeper falloff for the forecast q_r field. The estimated exponent with fit uncertainty is $H = 0.65 \pm 0.05$.

Over the 1-h sequence of images analyzed, H varied from 0.53 to 0.69, with a mean value of 0.55 ± 0.03. Here, H was insensitive to the values of the upper and lower bounds placed on the reflectivity within the ranges mentioned at the end of section 2c. This exponent is used to differentiate fractionally the fields for the moment-scale analysis, as described in the next section and the appendix.

c. *Moment-scale analysis*

Multiscale moments of any field φ are computed for a range of averaging scales r (higher r implies lower scale),

$$M_q(r) = \langle |\varphi_r(x, y)|^q \rangle, \tag{6}$$

where φ_r represents field values at scale r, q is the order of the moment, and $\langle\ \rangle$ denotes the average over all the pixels of scale r in an image. Note that the reason for introducing the notation φ is to distinguish the field used in moment-scale analysis from the observed field R, such as rainfall or RLW, for reasons explained below. The scale of the image typically is dyadically reduced from its original (highest) resolution by successive spatial averaging of the field by a factor of two at each step. Notice the fundamental difference between (4) and (6): (4) involves subsampling (i.e., differences) of the field at distances (lag) l apart; (6) involves averaging (i.e., integrating) the field over scales r. These two analysis methods therefore provide different information, as will become more apparent in what follows.

Moment-scale analysis gives information about the intermittency of a field, where the notion of intermittency is generalized beyond the often-used notion of zero intermittency (i.e., inhomogeneity of the ''rain–no rain'' structure). This more general concept of intermittency is one that is natural to multiscaling fields (e.g., Davis et al. 1996a), and refers to the varying degree of sparseness or inhomogeneity of different intensity levels. With this definition, one can see that higher intensity levels are more intermittent (sparse) than the lower intensities.

To interpret the results of moment-scale analysis, consider a highly intermittent and ''spiky'' field featuring highly localized peaks and sharp gradients. Degrading the resolution of the field will diminish the spikes because they are averaged with lower surrounding values. For moments of order $q > 1$, the averaging will thus result in reduced moments that lead to negative slopes on a plot of moment versus the averaging scale r. On the other hand, for a field that is considerably smoother, peaks are not so localized and averaging will have a lesser effect because intense values are more likely to be surrounded by other intense values. Thus the moment-versus-scale plots will be less steep for smoother fields.

Scaling of the moments occurs when

$$M_q(r) \sim r^{-K(q)}, \tag{7}$$

where $K(q)$ is the moment-scaling exponent function that, in practice, is estimated by log–log linear regressions of the qth moment of $|\varphi_r|$ versus r. It is clear that $K(1) = 0$, because the unconditional mean of the entire field is scale independent. Most scalar fields in

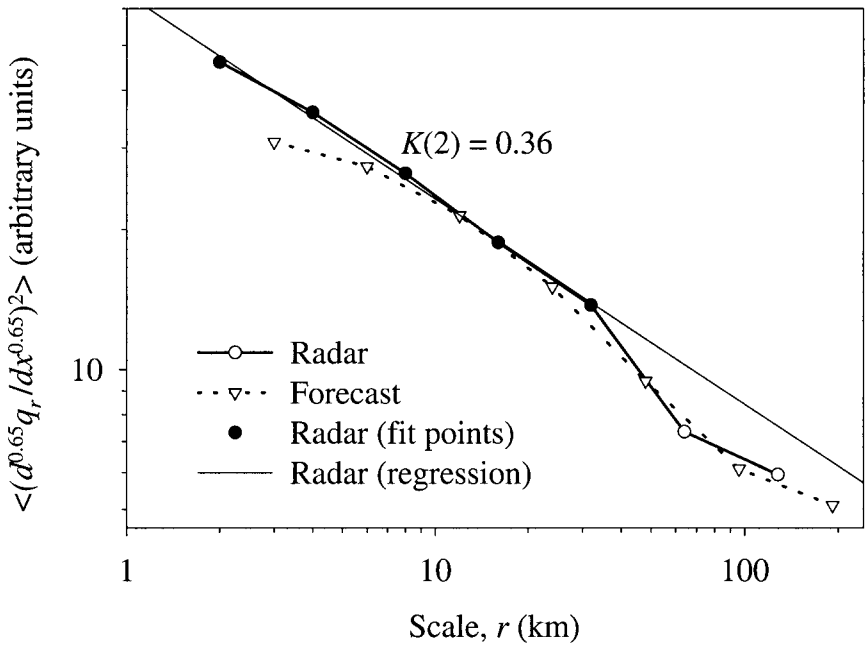

FIG. 5. Moment scaling ($q = 2$) for the fractionally differentiated ($H = 0.65$) forecast q_r field (dotted line–triangles) and the radar observed q_r field (solid line–circles). Comparison of the moments with averaging scale shows a leveling off for the forecast q_r field, indicating a falloff in the intermittency of higher values. The estimated slope with fit uncertainty is $K(2) = 0.36 \pm 0.01$ (see text for the selection of $H = 0.65$).

the geosciences, such as RLW in our case, do not show scaling of the moments; however, the increments or fluctuations do, and this is the reason for using the notation φ_r for the moment-scale analysis, because this analysis is often carried out on the fluctuations of the observed field and not the field itself. Equation (7) can be shown to be a property of multiplicative (multifractal) cascades [e.g., Gupta and Waymire (1993) and references there], which are popular in the phenomenological modeling of turbulence velocity fluctuations and precipitation fields.

A practical point to note is that the spectral slope β of a field is an indicator of whether the moment-scale analysis should be carried out on the field itself or on its fluctuations. In theory, it can be shown (Menabde et al. 1997) that the spectral slope β of a multiplicative cascade [i.e., one which is characterized by (7)] obeys $\beta_{\text{casc}} = D - K(2)$, where D is the geometrical dimension of the field (i.e., here $D = 2$). Because $K(2) > 0$, for a 2D spatial field one has $\beta_{\text{casc}} < 2$. Thus, only in the case of real fields with $\beta < 2$ should the moment-scale analysis be performed on the observed values [this is rare but nonetheless possible for rainfall, as discussed in Harris et al. (1996)]. If one wishes to adopt the moment-scale framework of analysis for an observed 2D field for which $\beta > 2$ (as found here), then the differentiation of the original field rather than the field itself must be used. It remains to determine what order of differentiation should be used for such a field.

There is a rich literature, largely promoted by Schertzer and Lovejoy (1987), that suggests the use of fractional gradients, with the order of fractional differentiation being the Hurst exponent, $H = \zeta(1)$. In a nutshell, the use of fractional derivatives in this manner stems from an analogy to the statistical properties of fully developed turbulence, and an extension of the techniques used to characterize turbulence to a wider range of geophysical phenomena. A background and an intuitive explanation of fractional differentiation are offered in the appendix.

One may think that by analyzing the moment scaling of the fractionally differentiated field of interest (i.e., RLW), one is effectively treating the real field as a fractionally integrated (i.e., a smoothed) representation of a cascade or field, which satisfies (7). One of the motivations to treat our field of interest in this way is that the use of cascades provides a framework of downscaling fields to a finer resolution with prescribed small-scale variability. As discussed in the introduction, introducing realistic small-scale variability via downscaling might provide a necessary and cost-effective alternative for rainfall–runoff modeling studies and rainfall retrieval from microwave radiometers.

Based on the arguments above, the H exponent, estimated at $H = 0.65$ from the observed field, is thus used to differentiate fractionally both the radar-observed and modeled RLW for the moment-scale analysis. The second moment as a function of averaging scale r for the fractionally differentiated radar-observed and modeled RLW fields in Fig. 1 is shown on the log–log plot in Fig. 5. The comparison shows that, for smaller scales,

the curve for the modeled field flattens out for $r < 12$ km, indicating comparatively less intermittency at these scales than for the radar-observed RLW field. This was found to hold for all moments $q > 0$, although scaling quality is usually poorer for very low order moments (e.g., $q < 0.5$), because the lower values are more influenced by noise (Harris et al. 1997). The scaling for the radar observations in the range from 2 to 32 km is very good, and for the entire sequence of images the slopes for the second-order moment-scaling exponent $K(2)$ ranged from 0.35 to 0.44, with a mean of $K(2) = 0.39 \pm 0.04$. There is some sensitivity to the upper and lower bounds placed on the reflectivity values. Lower bounds only had an effect for $q < 1$; the upper bounds had an effect for moments of $q \sim 2$ and above. Varying the upper bound between 50 and 55 dBZ increased $K(2)$ by about 0.02, and allowing complete hail contamination by increasing the bound to 60 dBZ increased $K(2)$ estimates by about 0.1. Higher-order moments were even more sensitive to hail contamination, increasing $K(3)$ from 0.75 to 1.00 and $K(4)$ from 1.44 to 1.90. A final point to consider concerns the specific values of scaling exponents [β, H, and $K(q)$] obtained in this study. The values are representative of the particular storm structure analyzed. In general one expects different storm conditions to result in different exponents, and a number of recent studies support this assertion. Harris et al. (1996) and a follow-up study (Purdy et al. 2001) found significant changes in scaling exponents as a result of changes in atmospheric stability and differences in the local orographic environment. In a similar way, Perica and Foufoula-Georgiou (1996a) found an empirical relation between their scaling exponents and the representative convective available potential energy of a storm.

4. Summary and conclusions

Of primary hydrologic importance with regard to the quality of a precipitation forecast is of course the magnitude of precipitation amounts, as well as the accuracy of the forecast time and location of the precipitating system. Efforts to improve these aspects of a numerical weather prediction model depend heavily on data assimilation methodologies and the improvement of physical model parameterizations. Reproducing precipitation variability of similar statistical structure as that observed has received less attention. However, adequate representation of precipitation variability has been demonstrated to be important for accurate estimation of hydrologic and energy fluxes (e.g., Ogden and Julien 1993, 1994; Winchell et al. 1998; Zhang and Foufoula-Georgiou 1997; Nykanen et al. 2001). Also, because precipitation interacts with the land surface in a complex nonlinear way and over a wide range of scales, it is important for numerical weather prediction models to reproduce the multiscale variability of precipitation and not only the precipitation variability over a single scale (e.g., the model resolution or the observations scale). This also becomes especially important in other applications of numerical cloud-resolving models, such as precipitation retrieval from microwave sensors, which were discussed in the introduction.

In a previous study, Zepeda-Arce et al. (2000) compared the multiscale rainfall variability of normalized rainfall fluctuations over scales of 12–48 km (using a 6-km model forecast) and over a duration of 12 h. That study found that, for the 7–8 May 1995 6-km forecast over Oklahoma, standardized rainfall fluctuations of the 18-min and hourly rainfall accumulation fields in the model had larger variability than in the observations but slower growth of variability with increase of scale. Also, the observations exhibited large temporal variability of their multiscale properties as the storm evolved, but the properties of the model remained almost constant. As discussed in the introduction, the methodologies employed in Zepeda-Arce et al. (2000) focused on rainfall fluctuations over scales of 12 km and larger.

In this study, a comparison of observed and model-produced precipitation fields (at 3-km resolution) is performed through the use of multiscale statistics such as Fourier analysis, structure functions, and moment-scale analysis, which allow interpretation of rainfall-intensity variability down to the resolution of the model. These statistical techniques revealed that the scale dependence of precipitation variability of the 3-km-resolution modeled fields was encouragingly similar to that observed by the radar, but only above a certain scale estimated at about 15 km. This is encouraging for the use of QPF estimates in many applications for which smaller-scale variability can be shown to be of minor importance. For scales smaller than about 15 km, however, the modeled variability falls off relative to radar-observed variability. The spectrum of the modeled fields showed a falloff in variability at high frequencies in comparison with the observed precipitation. The structure function was much steeper for the model, indicating a more spatially correlated structure than for the radar. Last, the moment-scale analysis showed a flattening out of the moment-scale curves, indicating a lack of intermittency, where intermittency refers to the sparseness of sharp intensities.

The falloff in variability of modeled precipitation at scales between the model resolution and approximately 5 times that scale is associated with (implicit) numerical diffusion and (explicit) computational-smoothing procedures inherent in the numerical model integration process, the latter of which is added to ensure numerical stability. Improving the spatial resolution will clearly improve the ability of the model to resolve small-scale features (e.g., Droegemeier et al. 1994, 1996; Lilly et al. 1998), but there always will be a falloff in variability at the smallest scales because of computational smoothing. The assertion that computational smoothing is a primary source of the lack in variability has been supported in previous work (Harris and Foufoula-Georgiou

2001) in which the variability at small scales was found to be related directly to the computational smoothing parameters.

The results of our study suggest that if one desires a 3-km precipitation forecast with an accurate representation of the scale dependence of precipitation variability at that scale and above, one may have to run the model with a horizontal spacing of about 600 m [i.e., 5-times smaller grid size than the desired scale of interest (3 km)]. This requirement is costly, if not infeasible, for the domain sizes typically needed to capture larger-scale forcings that influence storm dynamics. It also is completely infeasible for ensemble predictions and probabilistic forecasts. Of course, a viable and widely used alternative is nested gridding, but questions of grid size and the impact of outer-domain resolution have not yet been addressed fully.

Another alternative worth exploring is stochastic downscaling, which can be performed on a personal computer in a few seconds per image. Based on the results of this study, it is suggested that the model output aggregated to a scale approximately 5 times the model grid resolution and then stochastically downscaled back to the desired smaller scales can result in a more realistic representation of the small-scale rainfall variability. The statistical methods of analysis used in this study, in particular the scaling exponents estimated from the radar fields, can be used to construct a downscaling methodology using an appropriate multiplicative cascading process that matches the moment-scaling function $K(q)$ that is estimated from the radar data. A study investigating the merits of this approach for improving the accuracy of microwave remote sensing of precipitation is currently under way.

Acknowledgments. This work has been partially supported by the U.S. Weather Research Program (NSF Grant ATM-9714387), the NASA–TRMM Program (Grant NAG5-7715), and the NOAA/NASA GCIP Program (Grant NAG8-1519). We wish to thank the National Computation Science Alliance and the University of Minnesota Supercomputing Institute, without whose resources and technical assistance this project would not be possible. Last, we acknowledge discussions with Shaun Lovejoy and the comments and suggestions from Mathias Steiner and one other reviewer.

APPENDIX

Moment-Scaling Analysis and Fractional Derivatives

In analogy to fully developed turbulence for which one has, for velocity v,

$$|v(x + l) - v(x)| \sim \varepsilon^{1/3}(x)l^{1/3}, \tag{A1}$$

where ε is the conserved energy flux, which is a scale-invariant process, an approach found in the literature (e.g., Lovejoy and Schertzer 1995) is that there exists a ''conserved,'' albeit unknown, quantity (analogous to ε in turbulence) for precipitation or any other geophysical field. Denoting this quantity by $\varphi(x)$, it is sometimes called the underlying ''conservative'' field, (Schertzer and Lovejoy 1987) to draw the analogy to the conserved energy flux in turbulence. If one makes an implicit assumption that it too is scale-invariant [as $\varepsilon(x)$ is for turbulence, and which can later be verified to be true or false for $\varphi(x)$], then one has for a generic field R, with scaling structure function,

$$|R(x + l) - R(x)| \sim \varphi^a(x)l^H. \tag{A2}$$

Without loss of generality one can set a to unity, and H is the scaling exponent that determines the scale dependence of the first-order structure function of R.

In other words, $R(x)$ on its own is not expected to satisfy (7), but $\varphi(x)$ may be characterized by its scaling moments as given by (7). To isolate $\varphi(x)$, we use the property of a fractional derivative [e.g., Hilfer (1997); Gorenflo and Mainardi (1998) and references therein] in which, for H real, the operator

$$\frac{\partial^H}{dx^H} \sim \lim_{l\to 0} \frac{1}{l^H}. \tag{A3}$$

One then obtains for a field as in (A2),

$$\frac{\partial^H R(x)}{dx^H} \sim \varphi(x). \tag{A4}$$

What remains after fractional differentiation is the field $\varphi(x)$, which can be analyzed using the moment-scale analysis of (6) and the scale invariance of $\varphi(x)$, implying that the relation in (7) holds.

As outlined in section 3, in practice one estimates H from the structure function [(4)], and from (5) and (A2) one has that $\zeta(1) = H$. Note that fractional differentiation is reversible by fractional integration (e.g., Gorenflo and Mainardi 1998; Hilfer 1997), and so, in principle, one can retrieve an observed field R from φ to within a multiplicative normalization constant. In this way R can be seen to be a smoothed representation of φ.

Fractional differentiation and integration are most easily carried out in Fourier space (e.g., Davis et al. 1996a). If $\tilde{R}(k)$ is the Fourier transform of the (real valued) generic field R, then the inverse Fourier transform of $\tilde{R}(k)|k|^H$, $H > 0$, corresponds to fractional differentiation, and the inverse Fourier transform of $\tilde{R}(k)|k|^{-H}$, $H > 0$, corresponds to fractional integration.

REFERENCES

Brewster, K., 1996: Implementation of a Bratseth analysis scheme including Doppler radar. Preprints, *15th Conf. on Weather Analysis and Forecasting.* Norfolk, VA, Amer. Meteor. Soc., 92–95.

Christakos, G., 1992: *Random Field Models in Earth Sciences.* Academic Press, 458 pp.

Davis, A., A. Marshak, W. Wiscombe, and R. Cahalan, 1996a: Multifractal characterizations of intermittency in nonstationary geo-

physical signals and fields. A model based perspective on ergodicity issues illustrated with cloud data. *Current Topics in Nonstationary Analysis,* G. Treviño et al., Eds., World Scientific, 97–158.

——, ——, ——, and ——, 1996b: Scale invariance of liquid water distributions in marine stratocumulus. Part I: Spectral properties and stationarity issues. *J. Atmos. Sci.,* **53,** 1538–1558.

Droegemeier, K. K., 1997: The numerical prediction of thunderstorms: Challenges, potential benefits, and results from realtime operational tests. *WMO Bull.,* **46,** 324–336.

——, G. Bassett, and M. Xue, 1994: Very high resolution, uniform-grid simulations of deep convection on a massively parallel processor: Implications for small-scale predictability. Preprints, *10th Conf. on Numerical Weather Prediction,* Portland, OR, Amer. Meteor. Soc., 376–379.

——, ——, D. K. Lilly, and M. Xue, 1996: Does helicity really play a role in supercell longevity? Preprints, *18th Conf. on Severe Local Storms,* San Francisco, CA, Amer. Meteor. Soc., 205–209.

——, and Coauthors, 1999: The explicit numerical prediction of an intense hailstorm using WSR-88D observations: The need for realtime access to Level II data and plans for a prototype acquisition system. Preprints, *15th Int. Conf. on Interactive Information and Processing Systems (IIPS) for Meteorology, Oceanography, and Hydrology,* Dallas, TX, Amer. Meteor. Soc., 295–299.

——, and Coauthors, 2000: Hydrological aspects of weather prediction and flood warnings: Report of the Ninth Prospectus Development Team of the U.S. Weather Research Program. *Bull. Amer. Meteor. Soc.,* **81,** 2665–2680.

Georgakakos, K. P., A. A. Carsteanu, P. L. Sturdevant, and J. A. Cramer, 1994: Observation and analysis of midwestern rain rates. *J. Appl. Meteor.,* **33,** 1433–1444.

Gorenflo, R., and F. Mainardi, 1998: Fractional calculus and stable probability distributions. *Arch. Mech.,* **50,** 377–388.

Gupta, V., and E. Waymire, 1993: A statistical analysis of mesoscale rainfall as a random cascade. *J. Appl. Meteor.,* **32,** 251–267.

Harris, D., and E. Foufoula-Georgiou, 2001: Subgrid variability and stochastic downscaling of modeled clouds: Effects on radiative transfer computations and rainfall retrieval. *J. Geophys. Res.,* in press.

——, M. Menabde, A. Seed, and G. L. Austin, 1996: Multifractal characterization of rain fields with a strong orographic influence. *J. Geophys. Res.,* **101,** 26 405–26 414.

——, A. W. Seed, M. Menabde, and G. L. Austin, 1997: Factors affecting multiscaling analysis of rainfall time series. *Nonlinear Proc. Geophys.,* **4,** 137–156.

Hilfer, R., 1997: Fractional derivatives in static and dynamic scaling. *Scale Invariance and Beyond,* B. Dubrulle et al., Eds., Springer-Verlag, 53–62.

Hou, D., E. Kalnay, and K. K. Droegemeier, 2001: Objective verification of the SAMEX '98 ensemble forecasts. *Mon. Wea. Rev.,* **129,** 73–91.

Kessler, E., 1969: *On the Distribution and Continuity of Water Substance in Atmospheric Circulations. Meteor. Monogr.,* No. 32, Amer. Meteor. Soc., 84 pp.

Kummerow, C., and L. Giglio, 1994: A passive microwave technique for estimating rainfall and vertical structure information from space. Part I: Algorithm description. *J. Appl. Meteor.,* **33,** 3–18.

——, W. S. Olson, and L. Giglio, 1996: A simplified scheme for obtaining precipitation and vertical hydrometeor profiles from passive microwave sensors. *IEEE Trans. Geosci. Remote Sens.,* **34,** 1213–1232.

Lilly, D. K., and B. F. Jewett, 1990: Momentum and kinetic energy budgets of simulated supercell thunderstorms. *J. Atmos. Sci.,* **47,** 707–726.

——, G. M. Bassett, K. K. Droegemeier, and P. Bartello, 1998: Stratified turbulence in the atmospheric mesoscales. *Theor. Comput. Fluid Dyn.,* **11,** 139–153.

Lin, Y., R. D. Farley, and H. D. Orville, 1983: Bulk parameterization of the snow field in a cloud model. *J. Appl. Meteor.,* **22,** 1065–1092.

Lovejoy, S., and D. Schertzer, 1995: Multifractals and rain. *New Uncertainty Concepts in Hydrology and Water Resources,* A. W. Kundzewicz, Ed., Cambridge University Press, 61–103.

Menabde, M., A. W. Seed, D. Harris, and G. L. Austin, 1997: Self-similar random fields and rainfall simulation. *J. Geophys. Res.,* **102,** 13 509–13 515.

——, ——, ——, and ——, 1999: Multiaffine random field model of rainfall. *Water Resour. Res.,* **35,** 509–514.

Miller, M. W., 2000: The determination of usefulness of precipitation forecasts and probabilistic precipitation verification using SAMEX 1998 ensemble data. M.S. thesis, School of Meteorology, University of Oklahoma, 106 pp. [Available from School of Meteorology, University of Oklahoma, 100 East Boyd, Room 1310, Norman, OK 73019.]

Nykanen, D., E. Foufoula-Georgiou, and W. Lapenta, 2001: Impact of small-scale rainfall variability on larger-scale spatial organization of land–atmosphere fluxes. *J. Hydrometeor.,* **2,** 105–121.

Ogden, F. L., and P. Y. Julien, 1993: Runoff sensitivity to temporal and spatial rainfall variability at runoff plane and small basin scale. *Water Resour. Res.,* **29,** 2589–2597.

——, and ——, 1994: Runoff model sensitivity to radar rainfall resolution. *J. Hydrol.,* **158,** 1–18.

Perica, S., and E. Foufoula-Georgiou, 1996a: Linkage of scaling and thermodynamic parameters of rainfall: Results from midlatitude mesoscale convective systems. *J. Geophys. Res.,* **101,** 7431–7448.

——, and ——, 1996b: Model for multiscale disaggregation of spatial rainfall based on coupling meteorological and scaling descriptions. *J. Geophys. Res.,* **101,** 26 347–26 361.

Pielke, R. A., 1984: *Mesoscale Meteorological Modeling.* Academic Press, 612 pp.

Press, W. H., S. A. Teukolsky, W. T. Vetterling, and B. P. Flannery, 1992: *Numerical Recipes in C: The Art of Scientific Computing.* 2d ed. Cambridge University Press, 994 pp.

Purdy, J., D. Harris, G. L. Austin, A. W. Seed, and W. Gray, 2001: A case study of orographic rainfall processes incorporating multiscaling characterization techniques. *J. Geophys. Res.,* **106,** 7837–7846.

Schertzer, D., and S. Lovejoy, 1987: Physical modeling and analysis of rain and clouds by anisotropic scaling multiplicative processes. *J. Geophys. Res.,* **92,** 9693–9714.

——, and ——, 1991: Scaling non-linear variability in geodynamics: Multiple singularities, observables, universality classes. *Non-linear Variability in Geophysics: Scaling and Fractals,* D. Schertzer and S. Lovejoy, Eds., Kluwer, 41–82.

Shapiro, A., S. Ellis, and J. Shaw, 1995: Single-Doppler velocity retrievals with Phoenix II data: Clear air and microburst wind retrievals in the planetary boundary layer. *J. Atmos. Sci.,* **52,** 1265–1287.

Spencer, R. W., 1986: A satellite passive 37-GHz scattering-based method for measuring oceanic rain rates. *J. Climate Appl. Meteor.,* **25,** 754–766.

Venugopal, V., E. Foufoula-Georgiou, and V. Saposzhnikov, 1999: Evidence of dynamic scaling in space–time rainfall. *J. Geophys. Res.,* **104,** 31 599–31 610.

Weygandt, S. S., 1998: The retrieval of initial forecast fields from single Doppler observations of a supercell thunderstorm. Ph.D. dissertation, School of Meteorology, University of Oklahoma, 257 pp. [Available from School of Meteorology, University of Oklahoma, 100 East Boyd, Norman, OK 73019.]

Wilson, J., D. Schertzer, and S. Lovejoy, 1991: Physically based rain and cloud modeling. *Non-linear Variability in Geophysics: Scaling and Fractals,* D. Schertzer and S. Lovejoy, Eds., Kluwer, 185–208.

Winchell, M., H. V. Gupta, and S. Sorooshian, 1998: On the simulation of infiltration- and saturation-excess runoff using radar-

based rainfall estimates: Effects of algorithm uncertainty and pixel aggregation. *Water Resour. Res.*, **34,** 2655–2670.

Xue, M., K. K. Droegemeier, V. Wong, A. Shapiro, and K. Brewster, 1995: Advanced Regional Prediction System (ARPS) Version 4.0 user's guide. University of Oklahoma. [Available online at http://caps.ou.edu/ARPS/ARPS4.guide.html.]

——, ——, and ——, 2000: The Advanced Regional Prediction System (ARPS)—a multiscale nonhydrostatic atmospheric simulation and prediction model. Part I: Model dynamics and verification. *Meteor. Atmos. Phys.,* **75,** 161–193.

——, and Coauthors, 2001: The Advanced Regional Prediction System (ARPS)—a multiscale nonhydrostatic atmospheric simulation and prediction tool. Part II: Model physics and applications. *Meteor. Atmos. Phys.*, in press.

Yaglom, A. M., 1987: *Basic Results.* Vol. 1, *Correlation Theory of Stationary and Related Random Functions,* Springer-Verlag, 526 pp.

Zepeda-Arce, J., E. Foufoula-Georgiou, and K. Droegemeier, 2000: Space–time rainfall organization and its role in validating quantitative precipitation forecasts. *J. Geophys. Res.,* **105,** 10 129–10 146.

Zhang, S., and E. Foufoula-Georgiou, 1997: Subgrid-scale rainfall variability and its effects on atmospheric and surface variable predictions. *J. Geophys. Res.,* **102,** 19 559–19 573.